

Adaptive enhancement of sea-surface targets in infrared images based on local frequency cues

A. Onur Karalı, O. Erman Okman, and Tayfun Aytaç*

TÜBİTAK UEKAE-İLTAREN, Şehit Yzb. İlhan Tan Kışlası, 8 cad., 417 sok., TR-06800 Ümitköy, Ankara, Turkey

*Corresponding author: tayfun.aytac@iltaren.tubitak.gov.tr

Received September 25, 2009; accepted December 18, 2009;
posted January 7, 2010 (Doc. ID 117651); published February 25, 2010

Image enhancement is an important preprocessing step of infrared (IR) based target recognition and surveillance systems. For a better visualization of targets, it is vital to develop image enhancement techniques that increase the contrast between the target and background and emphasize the regions in the target while suppressing noises and background clutter. This study proposes what we believe to be a novel IR image enhancement method for sea-surface targets based on local frequency cues. The image is transformed blockwise into the Fourier domain, and clustering is done according to the number of expected regions to be enhanced in the scene. Based on the variations in the elements in any cluster and the differences between the cluster centers in the frequency domain, two gain matrices are computed for midfrequency and high frequency images by which the image is enhanced accordingly. We provide results for real data and compare the performance of the proposed algorithm through subjective and quantitative tests with four different enhancement methods. The algorithm shows a better performance in the detail visibility of the target. © 2010 Optical Society of America
OCIS codes: 100.2000, 100.2980, 110.3080, 330.1800, 110.3000.

1. INTRODUCTION

The processing of sea environments in an IR band is a challenging research subject because the sea radiance depends on sky reflections, sun glints, blackbody emissions from wave facets, and atmosphere [1]. Apart from the background clutter, low signal-to-noise ratio, low contrast, sensor noises, and the thermodynamic state of the targets affect the detection and visualization of the targets in the sea background or at the horizon. Therefore, for a successful target detection and a better visualization of high dynamic range (HDR) IR images, it is important to develop efficient enhancement techniques that increase the contrast between the target and background and emphasize target edges, while suppressing noises and the background clutter without introducing artifacts.

In image enhancement, the proposed solutions are case dependent; therefore, it is very difficult to develop an enhancement technique working well under different conditions. Similarly, there is no standard or metric for the performance comparison of the enhancement techniques [2]. In this study, we will focus on the IR images consisting of sea-surface targets. Many of the surveillance systems require intruder detection, threat detection approaching from the sea or horizon, and a better visualization of targets for classification and identification purposes. To the best of our knowledge, no attempt has been previously made to develop an IR image enhancement technique specific for sea-surface targets and to compare its performance with histogram and unsharp masking (UM) based methods. We propose an adaptive enhancement method based on the local frequency cues in the image. We show through subjective and quantitative tests that it performs well for the detail visibility in the target region.

This paper is organized as follows: Section 2 reviews

the state-of-the-art IR image enhancement techniques. In Section 3, the proposed algorithm is explained. The experimental results with a detailed discussion of the effects of the algorithm parameters on the performance are provided in Section 4. Subjective and quantitative comparisons are presented in Section 5 together with a brief description of the compared methods. The concluding remarks are made and directions for future research are provided in the last section.

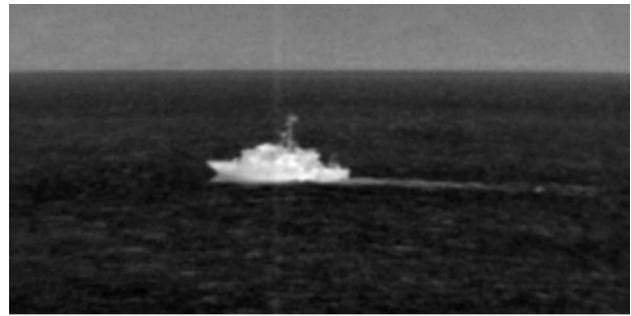
2. RELATED WORK ON IR IMAGE ENHANCEMENT

The image enhancement techniques can be generally divided into four categories, which are amplitude scaling, histogram modification, noise removal, and edge enhancement [2]. In an earlier work [3], contrast improvement techniques such as bit slicing, histogram equalization, and contrast improvement through look-up tables are used, together with noise reduction techniques, for image enhancement. The IR image sequences are enhanced by the motion estimation in [4–6]. The dynamic range enhancement is accomplished using a logarithmic image processing model in [7]. In [8], the effects of the IR image enhancement techniques on human based target detection are evaluated via psychophysical experiments. The authors implemented three different histogram modification techniques which are histogram projection, histogram equalization, and histogram weighted hybrid mapping and median filtering. In [9], the authors proposed a manual display mapping for a better visualization of 12–14 bit IR images in 8 bit displays. A two-stage IR image enhancement technique based on local and global contrast enhancement is proposed in [10]. They enhanced

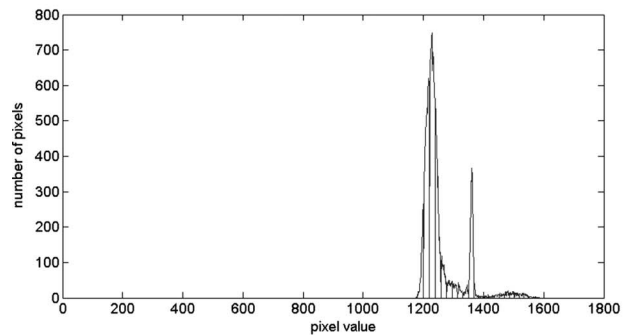
first global contrast by adaptive plateau histogram equalization (APHE) and then used adaptive gain control based on the wavelet transform for the local contrast enhancement. A tail-less version of the APHE and a version of the UM method, method of Aare Mällo (MAM), are applied for the IR image enhancement in [11]. In [12], an adaptive contrast enhancement method based on the wavelet transform is proposed. A local area processing method based on histogram shaping and the adaptive Wiener filtering for noise removal are used for the contrast enhancement in [13]. The adaptive unsharp masking (AUM) technique is proposed in [14] for the image enhancement. A quantitative assessment of the UM method in x-ray fluoroscopy is made in [15]. In [16], the edges are enhanced by adaptive thresholding using the error-diffusion algorithm. The authors implemented a spatiotemporal homomorphic filtering technique using a qualitative model for the far IR scenes in [17]. An adaptive version of the same method is proposed in [18]. The IR images are enhanced using the autoregressive moving average filter and H_∞ bounds in [19]. In [20], an anomalous frequency is detected using Fourier transform along the column in the image block and inverse Fourier transform is applied to the thresholded frequency for enhancement. The IR image enhancement based on a human visual system is proposed in [21] using the multifractal theory. Balanced contrast limited adaptive histogram equalization and contrast enhancement (BCLAHE-CE) techniques are used together for an improved visualization of the IR images in [22]. An evaluation is performed through a subjective analysis based on human observers. It outperforms the histogram equalization, Fattal's method [23], and the retinex algorithm [24] in the subjective tests. In [25], a bilateral filter is used for the dynamic range compression of the IR HDR images and the proposed algorithm is compared with the histogram equalization and retinex algorithm. In our earlier work [26], we made a comparative analysis of the different IR image enhancement techniques for sea-surface targets. It is observed that the BCLAHE-CE provides good results for different scenarios in the subjective and quantitative tests among the compared methods.

3. PROPOSED IR IMAGE ENHANCEMENT METHOD

In this study, we are mainly interested in the enhancement of IR images consisting of sea-surface targets. An example image and its histogram are shown in Figs. 1(a) and 1(b), respectively. As shown in Fig. 1(b), the histogram has a three modal distribution, where the first and second parts of the distribution correspond to the sea and sky regions, respectively. They have intensity values ranging approximately between [1180,1280] and [1350,1370]. The third part of the distribution having greater intensity values ranging approximately between [1440,1560] corresponds to the target. Our aim is to emphasize the target regions and detail level in the target without introducing an undesirable artifact and increasing the noise level in the image. We propose an adaptive method based on local frequency cues (AMLCF). The pro-



(a)



(b)

Fig. 1. (a) Sample image and (b) its histogram.

posed method has two stages: local clustering in the frequency domain and image enhancement.

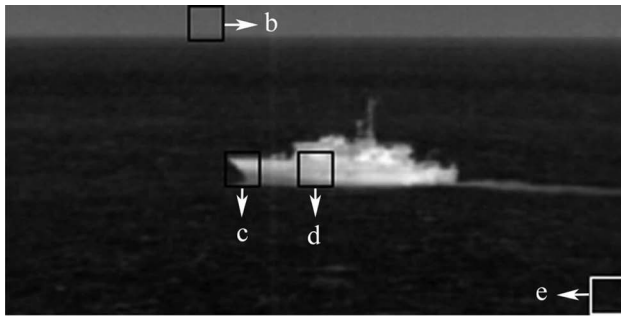
According to this method, first of all, an image of size $M \times N$ is divided into blocks at a specified size $B_1 \times B_2$ and the discrete Fourier transform (DFT) of each block is computed. The evaluated DFT coefficients are then used to cluster these blocks according to their frequency domain characteristics which are the key features used to discriminate the regions to be enhanced. In fact, the motivation at this point is to enhance the high frequency components as suggested by the method of UM [27]. On the other hand, the enhancement procedure is applied to the decided possible target regions with higher gain which makes the details of the image more visible but especially inside the target. For this purpose, the image is passed through appropriate filters and a low-pass, a mid-pass, and a high-pass image are obtained with a size of $M \times N$. Then, two $M \times N$ matrices, one of which is used to enhance the mid-pass while the other one is used to enhance the high-pass image, are elementwise multiplied by the mid-pass and high-pass images, respectively. Each element of those matrices is evaluated according to the three different attributes listed as follows:

- frequency characteristics of the cluster that the element is included;
- similarity between the frequency characteristics of the block that the element is included and the frequency characteristics of the corresponding cluster;
- distance between the spatial location of the element and the center points of the blocks.

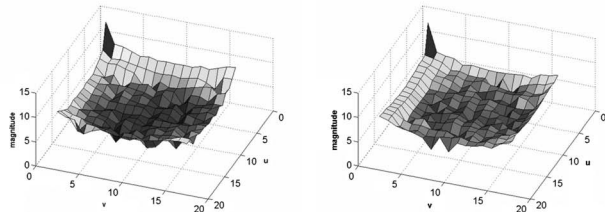
The first two factors are for realizing our main motivation of adaptive frequency selective enhancement while the last factor is for removing the blocking artifacts caused by the proposed procedure. Finally, using the low-pass image and the enhanced mid-pass and high-pass images, the resultant enhanced image is reconstructed. The details of the algorithm are explained in the subsequent sections.

A. Clustering in Frequency Domain

The target, sea, and sky regions have different frequency contents due to their textures. The sea surface usually consists of wave reflections with an additive noise and the sky has a gradual intensity distribution with noise added on it. The frequency distribution in the target regions differs from the sea and sky transitions due to its shape. Fourier transforms of the blocks corresponding to the target, target-sea transition, sea surface, and sky [Fig. 2(a)] are shown in Figs. 2(b)–2(e), respectively. As seen from the figure clearly, the four parts of the IR scene have dif-

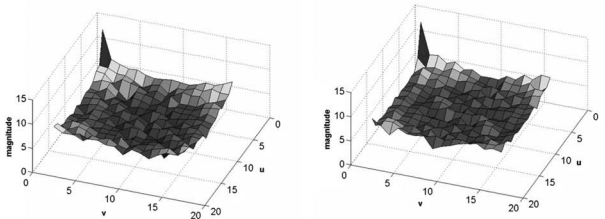


(a)



(b)

(c)



(d)

(e)

Fig. 2. Fourier transform of the blocks given in (a): (b) target (c) target-sea transition, (d) sea, and (e) sky.

ferent frequency characteristics, ranking from low to high as sea surface, sky, target, and target-sea transition, which is our main motivation in choosing the local frequency clustering approach.

The images to be enhanced have HDR characteristics. The local frequency clustering operations are done using these HDR images. For each block, Fourier transform is computed by the equation below:

$$F_i(u, v) = \frac{1}{B_1 B_2} \sum_{x=0}^{B_1-1} \sum_{y=0}^{B_2-1} I_i(x, y) e^{-j2\pi[(ux/B_1)+(vy/B_2)]}, \quad (1)$$

where $I_i(x, y)$ and $F_i(u, v)$ are the i th block of the image and its Fourier transform, respectively. Then, the absolute value of the 2-D frequency distribution of each block is converted to a vector V_i by zigzag scanning. As the Fourier transform is symmetric for real data, we use only half of it. Therefore, the length of V_i is $B_1 B_2 / 2$. The Euclidian distances between these arrays, d , as given in Eq. (2), are used to construct a hierarchical cluster tree and the clustering is done using this tree with respect to the nearest distance [28],

$$d_{rs}^2 = (V_r - V_s)(V_r - V_s)^T. \quad (2)$$

The maximum number of clusters c is a parameter and is set according to the number of regions to be enhanced. The clustering result for the image shown in Fig. 1(a) is given in Fig. 3 for $c=6$. As a result of the clustering process, each block of the image is assigned to a cluster. A cluster center CC is calculated by averaging the V_i 's. The computed cluster centers for the same image are shown in Fig. 4. These cluster centers are sorted according to the in-cluster frequency distribution. The vectors corresponding to each cluster center are normalized with the energy of that cluster in overlapping windows of size 3 to find the normalized cluster centers \overline{CC}_j 's, whose n th element is evaluated by the equations below:

$$TE_j = \sum_{n=1}^{B_1 B_2 / 2} [CC_j(n)]^2, \quad (3)$$

$$\overline{CC}_j(n) = \frac{[CC_j(n-1)]^2 + [CC_j(n)]^2 + [CC_j(n+1)]^2}{TE_j}, \quad (4)$$

where j represents the cluster number ranging from 1 to c ; TE_j is the energy of the j th cluster center CC_j . Then, the weights for each cluster center are defined as in Eq. (5),

$$w_j = \sum_{n=1}^{B_1 B_2 / 2} \overline{CC}_j(n). \quad (5)$$

These weights are used to sort clusters from high to low according to their frequency components and as a gauge to show inter-cluster distances. The blocks in the cluster with the highest cluster center weight are assumed to be in the target region whereas those in the cluster that have the smallest cluster center weight are assumed to be the background. In addition, the gains assigned to each block center are derived from the corresponding w_j . This process will be explained in the next section.

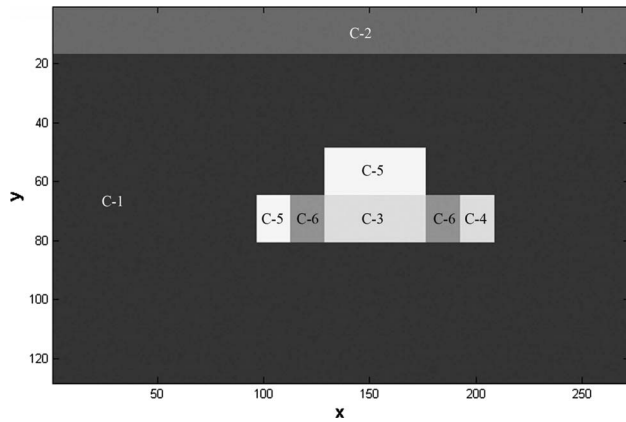


Fig. 3. Distribution of the image blocks according to their clusters.

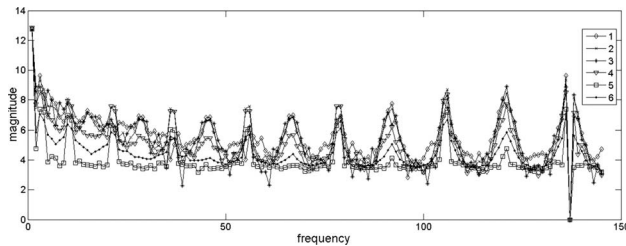


Fig. 4. Cluster centers.

B. Enhancement

A modified UM based adaptive enhancement technique is applied in the AMLFC. The UM based methods divide the original image into its low and high frequency images. The enhancement is usually done by the multiplication of the high frequency image with a constant to emphasize the details in the image [27]. However, with these methods, the background clutter is also enhanced at the same time due to the global implementation and halo effects occur around the hot targets [22].

In our method, on the other hand, by adjusting the gains with the help of the weights calculated according to the results of the frequency clustering stage, each midfrequency and high frequency component of the image blocks is enhanced with different gain coefficients. The halo effects are reduced by enhancing the two different frequency components properly.

1. Gain Matrix Generation

The midfrequency image consists of transitions in the target texture whereas the high frequency image consists of mostly Gaussian noises. So different gain factors for these two filtered images are defined to enhance the details of the target area while suppressing the noise in the image. Instead of multiplying the midfrequency and high frequency components of each block with a single gain coefficient, two different gain matrices are constructed for each image which has the same size as with the original image. Each pixel in the image has a different gain coefficient according to its spatial position and the frequency characteristics of the block it belongs to. Hence, the mul-

tiplication of the midfrequency and high frequency images with these gain matrices removes the blocking artifacts.

The gain matrix is computed by first assigning weights w to each block center according to the cluster to which that block belongs to as given in the following equation:

$$BW(k) = w_j, \quad k\text{th block} \in \text{cluster}_j, \quad (6)$$

where BW is the weight of the k th block and k changes from 1 to b , total number of blocks. Then, the distance from a single pixel to all block centers BC is computed using the equation below:

$$D_k(x,y) = \frac{1}{\sqrt{(BC_k(x_c) - x)^2 + (BC_k(y_c) - y)^2 + \epsilon}}, \quad (7)$$

where x_c and y_c are the coordinate centers of the block centers and ϵ is a small number (0.1 in our case) added to avoid an infinite multiplication coefficient at the weighted sum calculation.

The gain matrix $G(x,y)$ is constructed using the Euler distance from that pixel to the block centers and the weight of the corresponding block center as in Eq. (8),

$$G(x,y) = \frac{\sum_{k=1}^b D_k(x,y) BW(k)}{\sum_{l=1}^b D_l(x,y)}. \quad (8)$$

As can be seen from the formulations, while the distance between the pixel and the block center increases, the contribution of the weight of that block center in the calculation of that pixel's weight decreases. In Fig. 5, the gain matrix can be seen which is evaluated for the image given in Fig. 1(a). This matrix is mapped to the two different ranges and the two different gain matrices, G_{mid} and G_{high} , are constructed by the following equations:

$$G_{\text{mid}}(x,y) = \frac{(G(x,y) - G_{\text{min}})\alpha_{\text{mid}}}{(G_{\text{max}} - G_{\text{min}})} + \beta_{\text{mid}}, \quad (9)$$

$$G_{\text{high}}(x,y) = \frac{(G(x,y) - G_{\text{min}})\alpha_{\text{high}}}{(G_{\text{max}} - G_{\text{min}})} + \beta_{\text{high}}, \quad (10)$$

where G_{max} and G_{min} are maximum and minimum values of the gain matrix, α_{mid} and α_{high} are multiplicative coef-

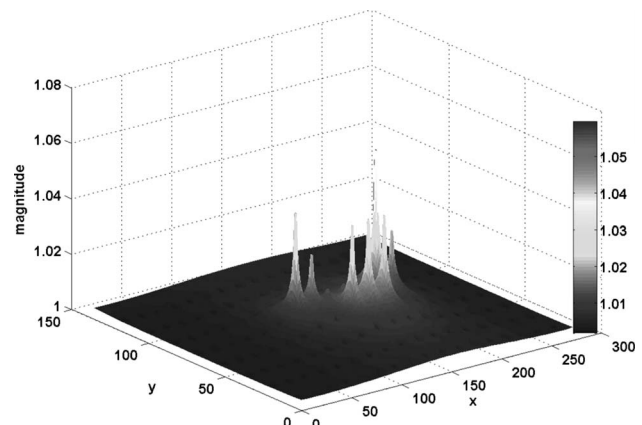


Fig. 5. Gain matrix.

ficients, and β_{mid} and β_{high} are the offset parameters for the midgain and high gain matrices, respectively. The parameters, β_{mid} and β_{high} are adjusted such that the enhanced images are not saturated. These parameters can be set by the user considering the scenario properties such as the noise level and the target size.

2. Construction of Low Frequency, Midfrequency, and High Frequency Images

The image is linearly mapped to the 8 bit dynamic range and low frequency, midfrequency, and high frequency components of the image are extracted from this image. This avoids extra linear mapping parameters for midfrequency and high frequency HDR images. The high frequency image (I_{high}) is extracted by first passing the original image from a 5×5 averaging filter and then subtracting the result from the input of the filter. The low frequency image (I_{low}) is extracted by passing the original image from a 25×25 averaging filter. The midfrequency image (I_{mid}) is obtained by subtracting the low and high frequency images from the original image.

3. Image Enhancement and Reconstruction

After defining and constructing the gain matrices and frequency components of the original image, elementwise multiplication between the midfrequency and high frequency images and their corresponding gain matrices is performed. At the next step, the resultant three images are added to obtain the enhanced image (I_{enh}) as described in the equation below:

$$I_{enh}(x,y) = I_{low}(x,y) + G_{mid}(x,y)I_{mid}(x,y) + G_{high}(x,y)I_{high}(x,y). \quad (11)$$

Then, the enhanced image is clipped between [0,255] intervals.

4. EXPERIMENTAL RESULTS

Sample images are extracted from IR videos recorded using longwave calibrated cameras of detector sizes [136,272] and [240,320] located on stabilized platforms. The field tests include targets of different sizes located at different distances and orientations from the observer. The targets at the horizon, multiple targets, and targets with land background are also considered.

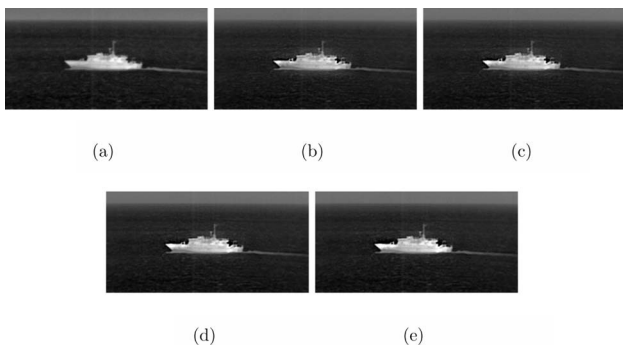


Fig. 6. (a) Original image and enhancement results ($\alpha_{high}=10$, $c=6$, $\beta_{mid}=\beta_{high}=0.5$, and $B_1=B_2=16$) for (b) $\alpha_{mid}=0.5$, (c) $\alpha_{mid}=1.5$, (d) $\alpha_{mid}=2.5$, and (e) $\alpha_{mid}=3.5$.

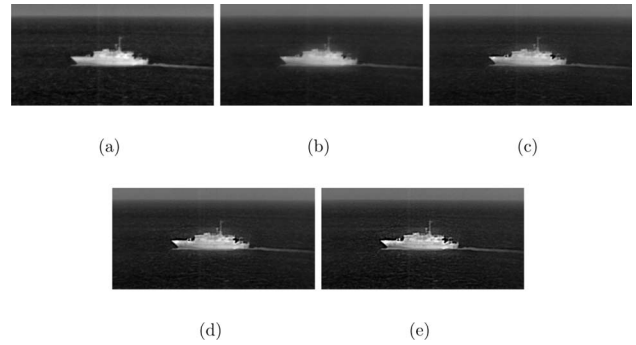


Fig. 7. (a) Original image and enhancement results ($\alpha_{mid}=0.5$, $c=6$, $\beta_{mid}=\beta_{high}=0.5$, and $B_1=B_2=16$) for (b) $\alpha_{high}=1$, (c) $\alpha_{high}=5$, (d) $\alpha_{high}=10$, and (e) $\alpha_{high}=15$.

The parameter α_{mid} is the multiplicative coefficient for the G_{mid} matrix used for contrast improvement in the target region and suppressing the reflections from the sea waves. The results obtained for different α_{mid} values are shown in Fig. 6. Small values of α_{mid} cause the truthfulness of the image to decrease while large values of α_{mid} cause the detail visibility of the target to decrease because intensity values in the target region saturate and the detail visibility of the target decreases.

Figure 7 shows the results obtained for different values of α_{high} , which is the multiplicative coefficient for the G_{high} matrix. The target details of the original image are enhanced because α_{high} increases the high frequency details in the target region. Non-target regions are affected less due to the structure of the gain matrix. While setting α_{high} more than unity results in an enhancement of the target edges and details, increasing α_{high} more saturates the image in the target region and the target details are lost.

The effects of different c values can be seen in Fig. 8. More clusters result in more transition blocks from the target region to the background. So bigger gain values spread to a wider region spatially around the target. It is more likely to merge the target with the horizon if the target size and the value of c are small. These parameters are modified by the user depending on the noise and target properties. During this work, it is observed that $c=6$ is large enough to segment the images properly in our data set.

The parameters β_{mid} and β_{high} are defined as the offset parameters of these two gain matrices and are chosen to

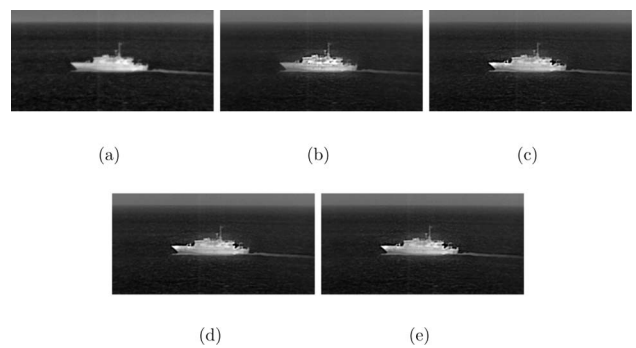


Fig. 8. (a) Original image and enhancement results ($\alpha_{high}=10$, $\alpha_{mid}=\beta_{mid}=\beta_{high}=0.5$, and $B_1=B_2=16$) for (b) $c=2$, (c) $c=4$, (d) $c=6$, and (e) $c=8$.

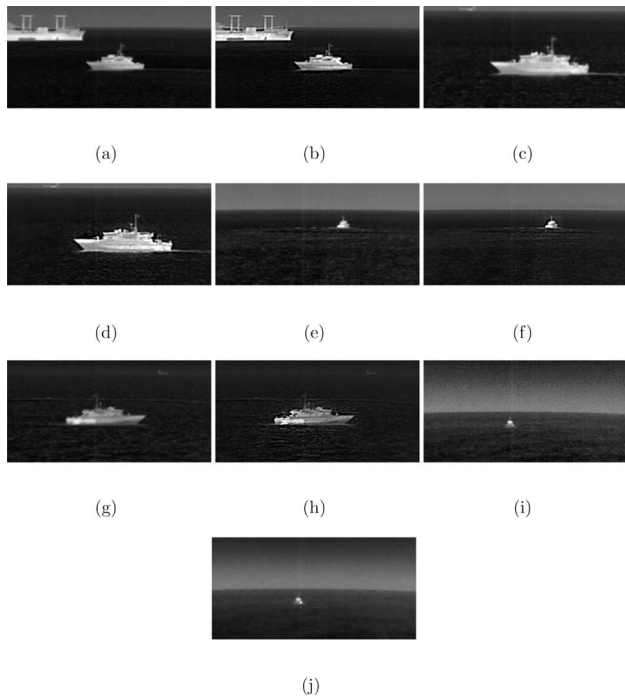


Fig. 9. [(a), (c), (e), (g), and (i)] Original images and enhancement results ($\beta_{\text{mid}}=0.5$) for (b) $\alpha_{\text{mid}}=1.5$, $\alpha_{\text{high}}=10$, and $\beta_{\text{high}}=0.5$, (d) $\alpha_{\text{mid}}=1.5$, $\alpha_{\text{high}}=10$, and $\beta_{\text{high}}=0.5$, (f) $\alpha_{\text{mid}}=0.5$, $\alpha_{\text{high}}=10$, and $\beta_{\text{high}}=0.5$, (h) $\alpha_{\text{mid}}=0.5$, $\alpha_{\text{high}}=10$, and $\beta_{\text{high}}=0.5$, and (j) $\alpha_{\text{mid}}=1.5$, $\alpha_{\text{high}}=2$, and $\beta_{\text{high}}=0.1$.

be less than 1 to suppress background clutter. The results for different scenarios are given in Figs. 9 and 10. In the results, the height and the width of the blocks are taken as 16. The parameters α_{mid} , α_{high} , β_{mid} , and β_{high} are adapted for different scenarios to obtain better results in terms of the visibility of the target details without introducing any artifacts. The high frequency noise suppression, wave glint removal, and target detail and edge enhancement are achieved for real data by adjusting the values of these parameters. For moderate midfrequency and high frequency suppressions in the sea and sky regions, β_{mid} and β_{high} are chosen as 0.5. In Fig. 9(i), a noisy image is seen and the high frequency noise suppression is

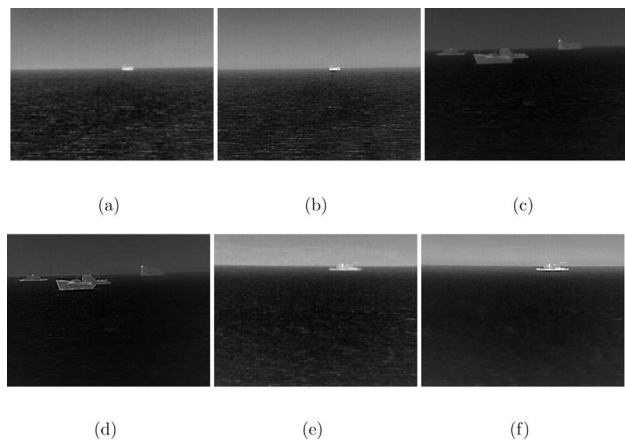


Fig. 10. [(a), (c), and (e)] Original images and enhancement results ($\beta_{\text{high}}=0.5$) for (b) $\alpha_{\text{mid}}=1.5$, $\alpha_{\text{high}}=10$, and $\beta_{\text{mid}}=0.5$, (d) $\alpha_{\text{mid}}=1.5$, $\alpha_{\text{high}}=10$, and $\beta_{\text{mid}}=0.5$, and (f) $\alpha_{\text{mid}}=0.5$, $\alpha_{\text{high}}=10$, and $\beta_{\text{mid}}=0.1$.

achieved in Fig. 9(j) by setting β_{high} to 0.1. A small target still exists without loss of detail or contrast. The effect of setting the value of β_{mid} to 0.1 is seen in Fig. 10(f), where the midfrequency components of the image are suppressed in the background region and wave glints are removed in the enhanced image.

5. COMPARATIVE ANALYSIS

In this section, the comparison of the proposed method with other well known techniques is presented based on subjective and quantitative tests. The compared algorithms are selected as APHE, BCLAHE-CE, MAM, and AUM. The first two methods are chosen because it has already found that they show good performance between the histogram based approaches [26]. The other methods are chosen for a fair comparison of the proposed method with other UM based methods. We believe that the choice of the algorithms will serve our comparison purposes.

A. Compared Algorithms

In adaptive thresholding, the nonzero elements of the histogram are found and smoothed using a median filter. The maximum gradients are computed using the difference between the subsequent elements of the filtered vector. The mean of the maximum gradients is taken as the threshold for the APHE. The original histogram is clipped below this threshold. The cumulative distribution function (CDF) of the modified histogram is computed and the original image is remapped using the modified CDF.

The BCLAHE-CE method integrates the process of dynamic range compression and local contrast enhancement. An operation on the image is given in the equation below:

$$I_{\text{enh}}(x,y) = p(I(x,y)) \left[\frac{I(x,y)}{I_{\text{low}}(x,y)} \right]^{\gamma}, \quad (12)$$

where p is the mapping function and γ is the contrast enhancement factor. The original histogram of the image is clipped to 1% of its total pixel number and excessive pixels are distributed over the entire image. This method is implemented locally by dividing the image into blocks and the equalization curve is constructed by the weighted averages of the curves for each block. A local implementation adapts the mapping function of the intensity image.

In the MAM, using the averaging filter and image subtraction, the image is separated into its low and high frequency bands. A linear scaling is applied to adapt the dynamic range of the low-pass filtered image. The high-pass image is enhanced as given in the following equation:

$$I_{\text{high}}(x,y) = \begin{cases} g_1 I_{\text{high}}(x,y), & |I_{\text{high}}(x,y)| < \nu \\ g_2 I_{\text{high}}(x,y), & |I_{\text{high}}(x,y)| \geq \nu, \end{cases}$$

where g_1 and g_2 are the two different gain coefficients and ν is the threshold value. Finally, low-pass and high-pass images are added and limited by a limiting factor to obtain the enhanced image.

In the AUM method, the local dynamic image is enhanced with respect to the local variance computed over 3×3 blocks. The gain is determined as

Table 1. Mean Scores of the Observers^a

	Original	AMLFC	APHE	BCLAHE-CE	MAM	AUM
Truthfulness	2.58	2.78	2.23	2.83	2.97	2.66
Target detail	2.37	3.07	1.73	2.90	3.02	2.55
Background detail	2.10	2.41	2.59	2.87	3.03	2.14
Artificiality	2.44	2.63	2.20	2.70	2.85	2.48
Total quality	2.48	2.82	2.19	2.85	2.95	2.56

^a1: Bad, 2: Poor, 3: Fair, 4: Good, and 5: Excellent.

$$\delta(x,y) = \begin{cases} 1, & V(x,y) < \tau_1 \\ \delta_{\text{mid}}, & \tau_1 \leq V(x,y) < \tau_2 \\ \delta_{\text{high}}, & V(x,y) \geq \tau_2, \end{cases}$$

where V is the local variance image and δ_{mid} and δ_{high} are gains satisfying the conditions $\delta_{\text{mid}} > 1$ and $1 < \delta_{\text{high}} < \delta_{\text{mid}}$. The thresholds τ_1 and τ_2 are chosen depending on the intensity distribution of the variance image. The enhanced image is computed as in Eq. (13),

$$I_{\text{enh}}(x,y) = \delta(x,y)I_{\text{high}}(x,y). \quad (13)$$

First, the output of the linear UM algorithm (I_{UM}) is computed as

$$I_{\text{UM}}(x,y) = I(x,y) + \lambda_x I_x(x,y) + \lambda_y I_y(x,y), \quad (14)$$

where I_x and I_y are the directional outputs of the Laplacian operator and λ_x and λ_y are the corresponding gains. In the adaptation, the error between the I_{enh} and I_{UM} is minimized with respect to gains λ_x and λ_y using the Gauss–Newton adaptation algorithm along the rows. The resulting image I_{UM} is taken as the enhanced image at the end of the iterations.

B. Subjective Tests

In the subjective tests, a similar way like in the study [22] is followed. 20 observers are asked to give points to the five different images based on the five different criteria. The criteria are the truthfulness of the image, detail visibility of the target and the background, unnatural artifacts, and total image quality. Each image appears randomly three times in the sequence, where a total of $5 \times 6 \times 3 = 90$ images are observed in a controlled office en-

vironment. In the evaluation, no information is given to the observers about the methods implemented and the original image. In the implementation, the tunable variables are determined by many trials and set to constants as they do not show large deviations for the images of similar characteristics in our database. In the implementation of the AMLFC, α_{high} is found to be 10 and α_{mid} , β_{mid} , and β_{high} are 0.5. For the BCLAHE-CE, γ is taken as 20. For the MAM, g_1 and g_2 are 3 and 2, respectively, and ν is set to 10. In the implementation of the AUM, the parameters are set as $\tau_1 = 200$, $\tau_2 = 500$, $\delta_{\text{mid}} = 5$, and $\delta_{\text{high}} = 2$.

The mean scores of the observers are given in Table 1. In the evaluation, the AMLFC has taken the highest point in the detail levels in the target. However, the slight difference between the detail levels of the target and the detail levels of the background due to the structure of the gain matrices results in a decrease in the points given to the truthfulness, background detail, and unnatural artifacts criteria. This affects the overall quality points given to the enhanced image obtained using the AMLFC. In the total quality, the MAM ranks first and the AMLFC and BCLAHE-CE have comparable scores. The mean score for the background detail is low for the AMLFC when compared to the BCLAHE-CE and the MAM because the proposed method suppresses the background clutter.

As an example, the results for an image evaluated in the tests are given in Fig. 11. As seen in Fig. 11(b), the AMLFC increases target details more when compared to the other methods. In this example, the effect of the clustering in the target enhancement can be clearly seen. The target at the right in this image is in the target region according to the clustering result whereas the target on the left hand side is clustered as a sea region. So, due to the gain matrices constructed depending on the clustering results, the edges and texture of the target at the right hand side are enhanced and the details of the other target are suppressed. We also note that the detail levels in the background around the target are kept.

C. Quantitative Tests

In the quantitative comparison, the contrast of the target is used as a performance metric. The contrast is computed for the images in a selected area of size $R \times S$ including the target using the formula in Eq. (15),

$$\text{contrast} = \sqrt{\frac{1}{RS} \sum_{x=0}^{R-1} \sum_{y=0}^{S-1} (I(x,y) - \bar{I})^2}, \quad (15)$$

where \bar{I} is the mean image in the selected region. The contrast results are given in Table 2 for the original and enhanced images. The best contrast is achieved using the

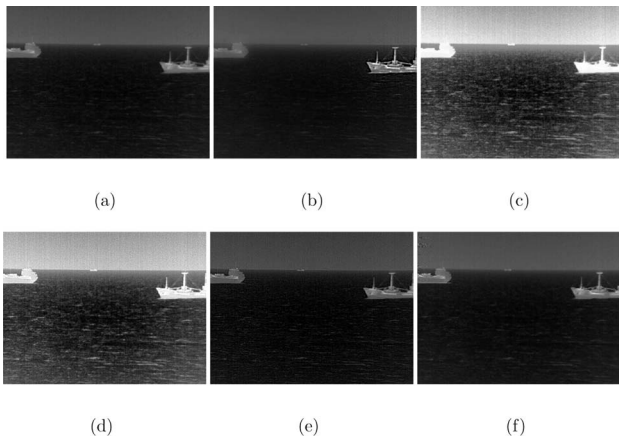


Fig. 11. Comparison results: (a) original image and enhanced images for (b) AMLFC, (c) APHE, (d) BCLAHE-CE, (e) MAM, and (f) AUM.

Table 2. Contrast Results in the Target Region

	Contrast
Original	50.70
AMLFC	65.56
APHE	64.27
BCLAHE-CE	64.58
MAM	43.90
AUM	53.56

AMLFC. The main reason for the high contrast value for the APHE method is that the target saturates after the enhancement. For this reason, the contrast metric is not valid for this algorithm because the APHE has the lowest score in the subjective tests. Although the MAM ranks good in the target detail score in the subjective tests, the contrast value is lower when compared to that of the AMLFC and BCLAHE-CE in the quantitative tests.

6. DISCUSSION AND CONCLUSION

In this study, we developed a novel IR image enhancement method based on local frequency cues. We discussed thoroughly the choice of algorithm parameters and showed the effectiveness of the algorithm with real data. Subjective and quantitative performance comparisons are made for different IR image enhancement techniques.

Although we have concentrated on the enhancement of specific targets, the results can be easily expanded to other IR images consisting of more cluttered backgrounds. For example, the sky may have broken clouds. The algorithm can handle these cases by properly adjusting the parameter c . As the clouds will have different textures when compared to a clear sky, sea surface, and sea-surface targets, they can successfully be segmented and beside targets, these broken clouds may also be enhanced. The algorithm performance does not depend on the perfect segmentation of the IR scene. However, if c is not chosen properly and the broken clouds have a high frequency distribution due to, for example, sun reflections, the algorithm may find the sea-surface targets as a part of the background and the sea-surface targets may not be enhanced properly.

The proposed algorithm is developed mainly to enhance the sea-surface target images obtained for the sea surveillance systems located on surface platforms. This imposes a limitation on the camera view angle. As the viewing angle and distance with respect to the sea-surface normal change, for example, in sky monitoring or airborne imaging applications, depending mainly on the sea-state, sun position, and atmosphere conditions, the radiance of the target and background will change. This will also affect the frequency distribution of the target and background. The proposed method may be extended to handle these types of scenarios by adjusting the internal parameters of the algorithm over large data sets.

In future studies, the parameters of the algorithm can be optimized using synthetic images at different atmospheric conditions, sea-surface reflections, and sea platform models. A real time application of the proposed algo-

rithm will also be considered. The proposed algorithm can also be accompanied with the existing target detection techniques in IR imaging systems to improve the processing time.

We believe that the results of this study will be useful for engineers and researchers designing IR imaging systems for sea-surface targets. While we have concentrated on IR imaging in the longwave, the technique proposed and compared with other methods in this paper may be useful for other IR wavelength intervals and also in a visible band.

ACKNOWLEDGMENTS

The authors would like to thank Dr. M. Alper Kutay for his support in this study, Özlem Türkçü for helpful discussions, Onur Jane for implementing the AUM method in his internship, and observers for joining in the subjective evaluations.

REFERENCES

1. C. R. Zeisse, C. P. McGrath, K. M. Littfin, and H. G. Hughes, "Infrared radiance of the wind-ruffled sea," *J. Opt. Soc. Am. A Opt. Image Sci. Vis* **16**, 1439–1452 (1999).
2. W. K. Pratt, *Digital Image Processing* (Wiley, 2001).
3. H. McCauley and J. E. Auburn, "Image enhancement of infrared uncooled focal plane array imagery," *Proc. SPIE* **1479**, 416–422 (1991).
4. J. C. W. Beck, "Image enhancement and moving target detection in IR image sequences," *Proc. SPIE* **2020**, 187–195 (1993).
5. M. Irani and S. Peleg, "Motion analysis for image enhancement: resolution, occlusion, and transparency," *J. Visual Commun. Image Represent.* **4**, 324–335 (1993).
6. W. Zhao and C. Zhang, "Scene-based nonuniformity correction and enhancement: pixel statistics and subpixel motion," *J. Opt. Soc. Am. A* **25**, 1668–1681 (2008).
7. M. Jourlin and J.-C. Pinoli, "Image dynamic range enhancement and stabilization in the context of the logarithmic image processing model," *Signal Process.* **41**, 225–237 (1995).
8. G. Aviram and S. R. Rotman, "Evaluating the effect of infrared image enhancement on human target detection performance and image quality judgment," *Opt. Eng. (Bellingham)* **38**, 1433–1440 (1999).
9. J. D. O'Connor, R. H. Vollmerhausen, and T. Corbin, "Performance evaluations of a manual display mapping method," *J. Electron. Imaging* **13**, 709–713 (2004).
10. M. Shao, G. Liu, X. Liu, and D. Zhu, "A new approach for infrared image contrast enhancement," *Proc. SPIE* **6150**, 1–6 (2006).
11. S. Weith-Glushko and C. Salvaggio, "Quantitative analysis of infrared contrast enhancement algorithms," *Proc. SPIE* **6543**, 1–12 (2007).
12. R. N. Strickland and H. I. Hahn, "Wavelet transform methods for object detection and recovery," *IEEE Trans. Image Process.* **6**, 724–735 (1997).
13. T. Pace, D. Manville, H. Lee, G. Cloud, and J. Puritz, "A multiresolution approach to image enhancement via histogram shaping and adaptive wiener filtering," *Proc. SPIE* **6978**, 1–11 (2008).
14. A. Polesel, G. Ramponi, and V. J. Mathews, "Image enhancement via adaptive unsharp masking," *IEEE Trans. Image Process.* **9**, 505–510 (2000).
15. K. N. Jabri and D. L. Wilson, "Quantitative assessment of image quality enhancement due to unsharp-mask processing in x-ray fluoroscopy," *J. Opt. Soc. Am. A* **19**, 1297–1307 (2002).

16. R. Eschbach and K. T. Knox, "Error-diffusion algorithm with edge enhancement," *J. Opt. Soc. Am. A* **8**, 1844–1850 (1991).
17. R. Highnam and M. Brady, "Model-based image enhancement of far infrared images," *IEEE Trans. Pattern Anal. Mach. Intell.* **19**, 410–415 (1997).
18. M. Tang, S. Ma, and J. Xiao, "Model-based adaptive enhancement of far infrared image sequences," *Pattern Recogn. Lett.* **21**, 827–835 (2000).
19. U. Qidwai, "Infrared image enhancement using H_∞ bounds for surveillance applications," *IEEE Trans. Image Process.* **17**, 1274–1282 (2008).
20. R. Muise and A. Mahalanobis, "Image enhancement for automatic target detection," *Proc. SPIE* **4726**, 267–272 (2002).
21. T. Yu, Q. Li, and J. Dai, "New enhancement of infrared image based on human visual system," *Chin. Opt. Lett.* **7**, 206–209 (2009).
22. F. Branchitta, M. Diani, G. Corsini, and A. Porta, "Dynamic-range compression and contrast enhancement in infrared imaging systems," *Opt. Eng. (Bellingham)* **47**, 076401 (2008).
23. R. Fattal, D. Lischinski, and M. Werman, "Gradient domain high dynamic range compression," in *Proceedings of the 29th Annual Conference on Computer Graphics and Interactive Techniques* (ACM Press, 2002), pp. 249–256.
24. B. Funt, F. Ciurea, and J. McCann, "Retinex in MATLAB," *J. Electron. Imaging* **13**, 48–57 (2004).
25. F. Branchitta, M. Diani, G. Corsini, and M. Romagnoli, "New technique for the visualization of high dynamic range infrared images," *Opt. Eng. (Bellingham)* **48**, 096401 (2009).
26. A. O. Karalı and T. Aytaç, "A comparison of different infrared image enhancement techniques for sea surface targets," in *Conference on Signal Processing, Communications and Applications* (IEEE, 2009), pp. 765–768.
27. R. C. Gonzalez and R. E. Woods, *Digital Image Processing* (Prentice-Hall, 2002).
28. R. O. Duda, P. E. Hart, and D. G. Stork, *Pattern Classification* (Wiley, 2001).